A Bjarne Saxhofs fond project

Development and validation of an in situ solar collector field test method

Weiqiang Kong, Simon Furbo and Bengt Perers

March 2019

Department of Civil Engineering Technical University of Denmark

Table of Contents

1. Introduction 1
2. Mathematical model 2
3. Shading model for solar collector field 4
   Identical solar collectors with the same slope 4
   Two different solar collectors with different slopes 5
   One fixed solar collector and one tracking solar collector 6
   Two tracking collectors 7
4. Incident angle modifier model 8
5. In situ test method 11
   Typical layout 11
   Array monitoring and field monitoring 12
   In situ test method 12
6. Experimental verification 13
   Case study 1 – Flat plate solar collector field in Sæby solar heating plant 13
   Case study 2 – Flat plate solar collector field in Tårs solar heating plant 18

Discussion 24

Conclusions 25

Acknowledgement 25

References 25

1. Introduction

Denmark has become the front runner in the solar heating plant market with large scale solar collector fields connected to district heating systems. Solar collector fields are composed of solar collectors connected in series and in parallel. An increasing number of large solar collector fields have been built in Denmark in the last years. 130 solar heating plants with a total solar collector area of 1,327,451 m² are in operation by the end of 2017 [1]. More solar collector fields are expected to be installed in the future. In Denmark, most of the solar collector fields are responsible for supplying heat to District Heating (DH) network. The typical supply temperatures are between 70 °C and 85 °C while the return temperatures are between 35 °C and 45 °C. The guaranteed thermal performance of solar collector fields is important for both solar heating plants owners and consumers. But a mismatch between solar energy input and heat demand can be anticipated. Solar irradiance fluctuates a lot during a day especially in the Nordic countries and meanwhile the thermal hysteresis of solar collector field is high which is mainly contributed by the large thermal capacitance of the solar collectors. A stable supply temperature for DH network is a big challenge for the operation strategy. Further, it is important that the thermal performances of solar collector fields can be predicted and that the performances are as high as expected.

However, there are few studies of theoretical models and in situ test methods suitable for solar collector fields. Further, so far no standards on thermal performance of collector fields are available. Thermal performance test methods and standards for single solar collectors have been developed for decades but they are quite different and cannot be directly used for solar collector fields. The knowledge and research of large solar collector field in situ tests is quite limited.

Federico Bava developed a detailed TRNSYS-Matlab model to simulate the behavior and thermal performance of a large solar collector field and then the simulated results were compared with measurements from a solar collector field in Høje Taastrup Denmark [2]. The results were good and acceptable. However, the TRNSYS model is a specific model for one solar collector field based on all the specific components simulation at the same time. It needs quite a big effort to build a new model from one existing model. Then the TRNSYS model is not flexible. It always has many restrictions such as simulation time step which cannot be arbitrarily changed.

PlanEnergi developed a Quasi - Dynamic model for simulation of large solar collector fields. The model was verified by comparison of 13 days' simulated and measured outlet temperature and energy output of the solar collector field in Løgum Kloster district heating plant [3]. It is a simple mathematical model and is easy to implement. However, the model has difficulties to simulate solar collector fields accurately in the morning.

In addition, improper layout and operation of large scale solar collector fields will reduce the solar heat production resulting in loss of money. Therefore, scientific research for large solar collector fields is needed. The aim of this project is to develop an in situ test method for large solar collector fields to predict and evaluate its thermal performance. By means of the test method, the quality and operation of solar collector fields can be secured and optimized.

Meanwhile, the standardization of the thermal performance prediction of large solar collector field is initiated recently by Denmark, Austria and China in ISO meetings [4]. Denmark was assigned as the leading

country. Therefore there is strong demand of research on solar collector fields both from industry and scientific institutions.

2. Mathematical model

The mathematical model is specially developed for testing and predicting the thermal performance of solar collector fields in solar heating plants.

The basic assumption of the in situ testing method is that the monitored solar collector row, or rows, or the whole solar collector field is assumed as a large single solar collector.

Other assumptions are summarized as follows:

- The collector row/rows/whole collector field (aperture/gross) area is the sum of all collectors' (aperture/gross) area
- The pipe heat losses are not modeled and will be compensated to/considered as part of the collector field heat losses
- The volume flow rate per square meter collector in the solar collector field is the same
- The orientation of each solar collector is the same
- The slope of each solar collector is the same.

The Quasi-Dynamic Test (QDT) model [5, 6] is widely used for single solar collector testing and the QDT test method was accepted as an international test standard [7]. The mathematical model of in situ test method is developed based on the modified QDT model, which is shown in Eq. (1). The meaning of each symbol is listed below.

$$q_u = \eta_{0,b} K_b\left(\theta_L, \theta_T\right) S_b G_b + \eta_{0,b} K_d S_d G_d - a_1(T_f - T_a) - a_2(T_f - T_a)^2 - a_3 u(T_f - T_a) + a_4(E_L - \sigma T_A{}^4) - a_5 dT_f / dt - a_6 uG \quad (1)$$

- q_u is the useful thermal output of solar collector field, W/m²
- $K_b(\theta_L, \theta_T)$ is incidence angle modifier for beam radiation, -
- K_d is incidence angle modifier for diffuse radiation, -
- θ is the incidence angle for direct radiation, °
- θ_L is the incidence angle in the longitudinal plane, °
- θ_T is the incidence angle in the transversal plane, °
- $\eta_{0,b}$ is peak collector efficiency, based on beam irradiance G_b -
- S_b is the shading coefficient for beam radiation, -
- S_d is the shading coefficient for diffuse radiation, -
- a_1 is the heat loss coefficient of solar collector at ambient temperature, W/(m²K)

- a_2 is the temperature dependence of heat loss coefficient of solar collector, W/(m²K²)
- a_3 is wind speed dependence of the heat loss coefficient, J/(m³K)
- a_4 is sky temperature dependence of the heat loss coefficient, -
- a_5 is the thermal capacity of the collector, J/m²K
- a_6 is wind dependence in zero loss efficiency, s/m
- T_f is the mean solar collector fluid temperature, °C
- T_a is the ambient air temperature, °C
- T_A is absolute ambient air temperature, K
- G_b is the beam irradiance on the collector, W/m²
- G_d is diffuse radiation on the collector, W/m²
- G is hemispherical solar irradiance on the collector, W/m²
- u is wind speed, m/s
- E_L is longwave irradiance (λ > 3 μm), W/m²
- σ is Stefan-Boltzmann constant, W/(m²K⁴)
- t is time, s

The left hand side of Eq. (1) is the useful heat output produced by solar collector field. The right hand side terms are collector field absorbed solar energy from beam irradiance, collector field absorbed solar energy from diffuse irradiance, the first order heat loss, the second order heat loss, the wind depended heat loss, the long-wave radiation heat loss, the transient energy term related to thermal capacity and the wind dependent heat loss in zero loss efficiency.

The mathematical model applies to a wide range of collector types in the field. But of course the investigated collector field should have the same collector type, like flat plate collector or parabolic trough collectors. The flat plate collectors with and without a foil are treated as the same type collector. The heat loss terms in Eq. (1) are not necessarily all used according to different collector types. For example, for glazed solar collector the long-wave heat loss is not significant and can be neglected in the calculation. If there is no wind speed measurements or negligible wind effect, the wind heat loss terms can be eliminated.

The in situ test mathematical model is almost the same as the QDT mathematical model except the shading effect added. The QDT model is mainly used for single solar collector testing which has no shading problem both in indoor and outdoor testing. The solar collector field is composed by many single solar collectors connected in rows and columns. Except the first row, shadings from the front rows always exist. Therefore, the parameters S_b and S_d are added in the model which is intended to describe the shading effect in the solar collector field. The detailed mathematical model for S_b and S_d can be seen in section 3. In addition, the incident angle modifier could also be different when concentrating collectors are used or

other non-symmetrical incident angle effects are known. The detailed solution methods are described in section 4.

3. Shading model for solar collector field

In a solar collector field, deploying the same type solar collectors with the same collector slope is the most common case. However, for some special cases, the solar collector deployment could be different. In this section the detailed shading models for different solar collector deployments are developed.

Identical solar collectors with the same slope

This is the most common case in most of the solar collector field. The front and back rows are composed of the same type solar collectors with the same slope. The simplified shading diagram for this case is shown in Fig. 1. The two identical collectors is represented by the two dark blue lines with the slope of β. H_{coll} is the width of solar collector. The dotted red line is the sunlight that just passes through the top of the front collector and irradiates on the surface of the back collector. Therefore, the dotted red line divides the back collector into two parts. The upper part of the collector can receive solar irradiance while the lower part, which is drawn as the light blue line (*Lshad*), is shaded from the sunlight. CC_{row} is the distance between the two solar collectors. The angle α_p generated by the sunlight and the horizon is the profile for beam shading angle while the angle α_g is the diffuse shading angle.

The shaded part of the back solar collector, *Lshad*, was derived by geometric calculation, which is finally shown as Eq. (2). The process of the derivation is omitted. Then the beam shading parameter S_b is obtained by knowing the *Lshad*, which is shown in Eq. (3). The diffuse shading parameter S_d can be calculated by Eq. (4).

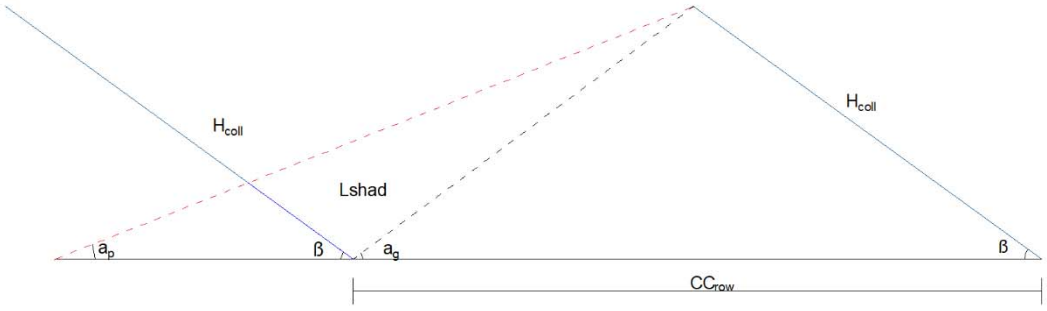

Fig.1: shading diagram for two identical solar collectors with the same slope

$$Lshad = \frac{\sin(\alpha_p)}{\sin(180 - \alpha_p - \beta)}\left(H_{coll}\frac{\sin(\beta)}{\tan(\alpha_p)} + H_{coll}\cos(\beta) - CC_{row}\right) \quad (2)$$

$$S_b = 1 - Lshad / H_{coll} = 1 - \frac{\sin(\alpha_p)}{\sin(180 - \alpha_p - \beta)}\left(\frac{\sin(\beta)}{\tan(\alpha_p)} + \cos(\beta) - \frac{CC_{row}}{H_{coll}}\right) \quad (3)$$

Where,

$$\alpha_p = \text{atan}[\frac{\tan(\alpha_h)}{\cos(\alpha_s - \alpha_{coll})}]$$

$$S_d = G_{dhoris}[1+\cos(\beta+\alpha_g K_{korr})]/2 + G_{horis}\rho_{ground}[1-\cos(\beta-\alpha_g K_{korr})]/2 \quad (4)$$

Where,

$$\alpha_g = \text{atan}(\frac{H_{coll}\sin(\beta)}{CC_{row} - H_{coll}\cos(\beta)})$$

- α_s is the solar azimuth, °
- α_{coll} is the solar collector azimuth, °
- α_h is the solar altitude, °
- G_{dhoris} is the diffuse solar irradiance on horizontal, W/m^2
- G_{horis} is the global solar irradiance, W/m^2
- ρ_{ground} is the ground reflectance, -
- K_{korr} is the diffuse shading severity (1.0 is the worst case), -

Two different solar collectors with different slopes

There could be another case that the solar collectors at the front and the back rows are different, even with different slopes. The shading diagram is shown in Fig. 2. The H_{coll1} and H_{coll2} represent the width of the front and the back solar collectors. β_1 and β_2 are the collector slopes respectively. In this case, the *Lshad,* S_b and S_d are derived as Eqs. (5-7).

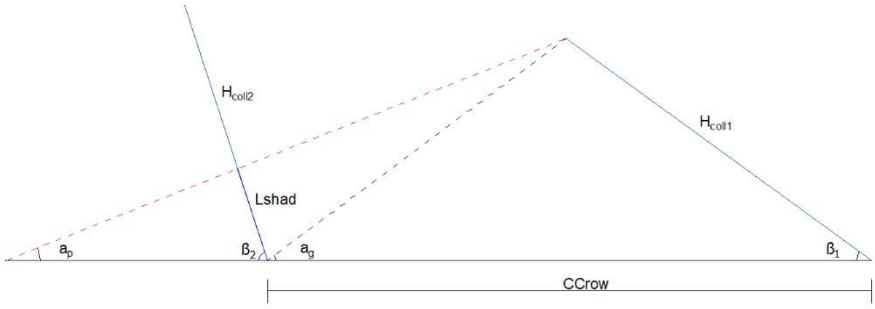

Fig.2: shading diagram for two different solar collectors with different slopes

$$Lshad = \frac{\sin(\beta_1)H_{coll1} + \cos(\beta_1)\tan(\alpha_p)H_{coll1} - CC_{row}\tan(\alpha_p)}{\sin(\beta_2) + \cos(\beta_2)\tan(\alpha_p)} \quad (5)$$

$$S_b = 1 - Lshad / H_{coll2} \quad (6)$$

$$S_d = G_{dhoris}[1+\cos(\beta_1+\alpha_g K_{korr})]/2 + G_{horis}\rho_{ground}[1-\cos(\beta_1-\alpha_g K_{korr})]/2 \quad (7)$$

The above two cases are mainly developed for the shading effect of fixed solar collectors, which are suitable for most cases of solar collector fields. However, there could be other cases existing, for example, tracking solar collectors with fixed solar collectors or only tracking solar collectors. The detailed shading model are also developed for these special conditions as follows.

One fixed solar collector and one tracking solar collector

The general shading concept of one tracking solar collector and one fixed solar collector is shown in Fig. 3. The tracking solar collector has a height of L_p from the ground to the rotating point. The collector may also have a depth of d from the rotating point to the surface. The width of tracking solar collector is H_{21} plus H_{22}, which is not necessarily the same. The collector slope β_2 is of course changing from time to time by tracking the sun. H_1 is the width of the fixed solar collector and β_1 is the fixed slope. CC_{row} is the distance between the two collectors. It can be measured from the middle of the fixed collector to the stand column of the tracking collector.

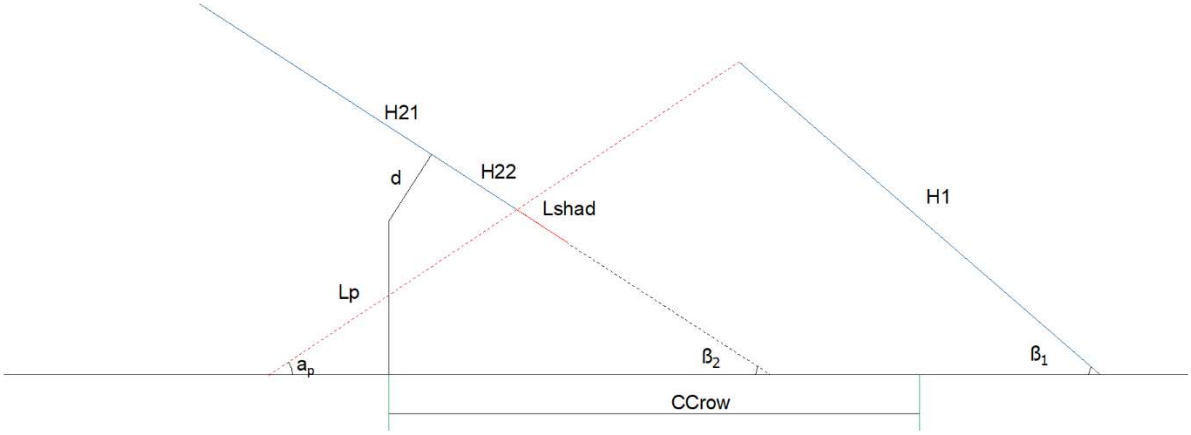

Fig. 3: Shading diagram for one tracking solar collector and one fixed solar collector

$$Lshad = H_{22} - \frac{L_p + CC_{row}\tan(\alpha_p) - H_1\sin(\beta_1) - 0.5H_1\cos(\beta_1)\tan(\alpha_p) + d\cos(\beta_2) - d\sin(\beta_2)\tan(\alpha_p)}{\sin(\beta_2) + \cos(\beta_2)\tan(\alpha_p)} \quad (8)$$

The shading length *Lshad* is derived as Eq. (8). S_b and S_d have the same format as Eq. (6) and Eq. (7) which are not necessarily listed.

The special case of the shading effect between one tracking solar collector and one fixed solar collector occurs when d=0. The shading diagram is shown in Fig. 4. The *Lshad* equation is simplified as Eq. (9).

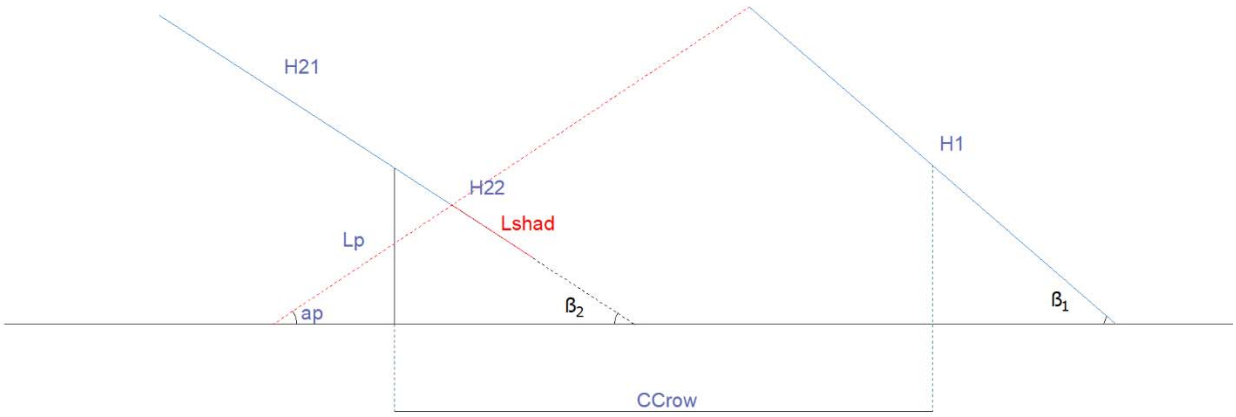

Fig. 4: Special case of shading diagram for one tracking solar collector and one fixed solar collector

$$Lshad = H_{22} - \frac{L_p + CC_{row}\tan(\alpha_p) - H_1\sin(\beta_1) - 0.5H_1\cos(\beta_1)\tan(\alpha_p)}{\sin(\beta_2) + \cos(\beta_2)\tan(\alpha_p)} \quad (9)$$

Two tracking collectors

The general shading geometry of two tracking solar collectors is shown in Fig. 5. The two solar collectors could have different collector lengths (H_{11}, H_{12}, H_{21}, H_{22}), different tracking slopes (β_1 and β_2), different column heights (L_{p1} and L_{p2}), and different collector depths (d_1 and d_2). The shade length *Lshad* is derived as Eq. (10). Similarly, S_b and S_d can use the same formula as Eq. (6) and Eq. (7).

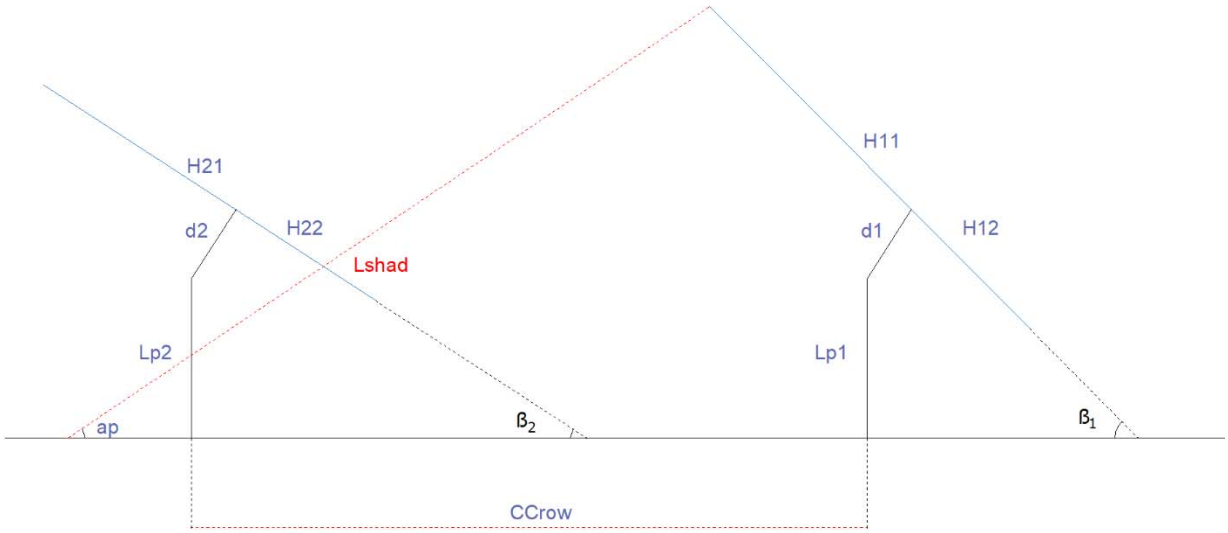

Fig. 5: shading diagram for two tracking solar collectors

$$Lshad = \frac{Hterm + L_p term + dterm + CC_{row} term}{\sin(\beta_2) + \cos(\beta_2)\tan(\alpha_p)} \quad (10)$$

Where,

$$Hterm = H_{11}[\sin(\beta_1) + \cos(\beta_1)\tan(\alpha_p)] + H_{22}[\sin(\beta_2) + \cos(\beta_2)\tan(\alpha_p)]$$

$$L_p term = L_{p1} - L_{p2}$$

$$dterm = d_1[\cos(\beta_1) - \sin(\beta_1)\tan(\alpha_p)] + d_2[\cos(\beta_2) - \sin(\beta_2)\tan(\alpha_p)]$$

$$CC_{row} term = CC_{row}\tan(\alpha_p)$$

The special case of the shading effect of two identical tracking collectors is $d_1=d_2$, $\beta_1=\beta_2$, $H_{11}=H_{21}$ and $H_{21}=H_{22}$ .The shading length *Lsahd* can be easily derived by simplifying Eq. (10), which is Eq. (11). Similarly, S_b and S_d can use the same formula as Eq. (6) and Eq. (7).

$$Lshad = H_{21} + H_{22} - \frac{CC_{row}\tan(\alpha_p)}{\sin(\beta) + \cos(\beta)\tan(\alpha_p)} \tag{11}$$

4. Incident angle modifier model

Incident Angle Modifier (IAM) is an important part for accurate prediction of the thermal performance of solar collector fields. Different solar collector types have different mathematical models for describing IAMs. For flat plate solar collectors, the b_0 equation or *tan* equation are accurate enough to model the IAM curve, which are shown as Eq. (12) and Eq. (13), where $K_b(\vartheta)$ is the incident angle modifier for beam irradiance, ϑ is the incident angle, b_0 and P are collector parameters that can be determined by testing.

$$K_b(\theta) = 1 - b_0\left(\frac{1}{\cos(\theta)} - 1\right) \tag{12}$$

$$K_b(\theta) = 1 - \tan^P\left(\frac{\theta}{2}\right) \tag{13}$$

For solar collectors like Evacuated Tubular Collector (ETC) and Compound Parabolic Collector (CPC), the incident angle effects are not symmetrical with direction of incidence. It is necessary to measure the incident angle effects from two perpendicular symmetric planes by the two separate incident angle modifiers, $K_b(\vartheta_L)$ and $K_b(\vartheta_T)$. The IAM is the product of the two separate IAM, see Eq. (14) [7].

$$K_b(\theta_L, \theta_T) = K_b(\theta_L, 0) \cdot K_b(0, \theta_T) \tag{14}$$

The longitudinal plane (index L) runs parallel to the optical axis of the collector, and the transversal plane (index T) is perpendicular to the optical axis. The angles ϑ_L and ϑ_T are the projections of the incident angle ϑ onto the longitudinal and transversal planes, respectively [7], see Fig. 6.

Typically, it is difficult to develop a brief mathematical model like Eq. (12) and Eq. (13) to describe the collector's IAM curve under different incident angles for non-symmetrical incident angle effects. Therefore, separate tests for $K_b(\vartheta_L)$ and $K_b(\vartheta_T)$ are needed. But the testing for $K_b(\vartheta_L)$ or $K_b(\vartheta_T)$ is usually

difficult and time consuming, especially for outdoor testing. For example, when $K_b(\vartheta_L)$ is determined, ϑ_T needs to be 0 during test period and several efficiency tests need to be carried out to get $K_b(\vartheta_L)$ under different values of ϑ_L.

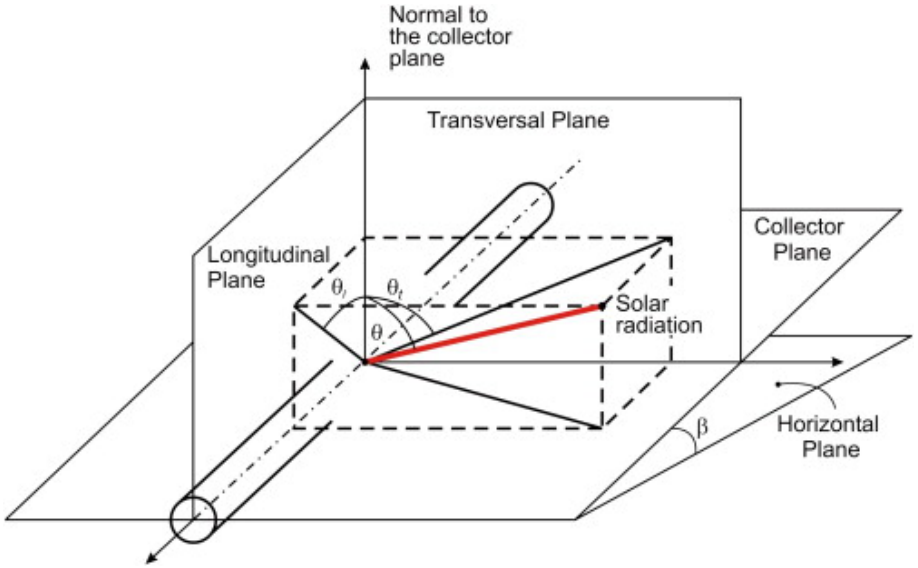

Fig. 6: Planes and angles relevant for determination of bi-axial IAM [8]

There are two other simpler ways to get accurate $K_b(\vartheta_L,\vartheta_T)$. One is using software like Tonatiuh [9], which is a Monte Carlo ray tracer for the optical simulation of solar concentrating systems. It can simulate the sunlight route and reaction to a certain shape of solar collector by knowing its geometry and materials' properties. The IAM of certain geometry collector can be calculated. This is a theoretical method for non-symmetrical IAM calculation, which is especially good for prototype concept solar collectors. Fig. 7 and Fig. 8 show one IAM example of a CPC solar collector. Fig. 7 is the 3D map of IAM versus both ϑ_L and ϑ_T while Fig. 8 shows 2D curves of IAM for different ϑ_L and ϑ_T. From the results a table can be made to give the accurate IAMs. The table can be used in the calculation of incident angle modifier for the mathematical model Eq. (1).

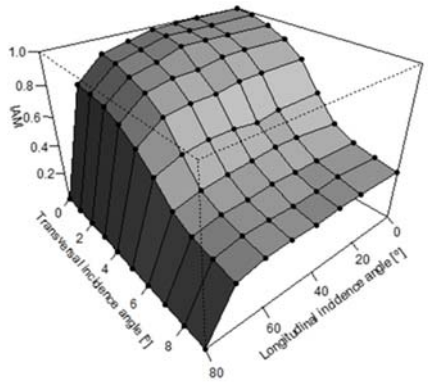

Fig. 7: IAM 3D map for a CPC solar collector by Tonatiuh

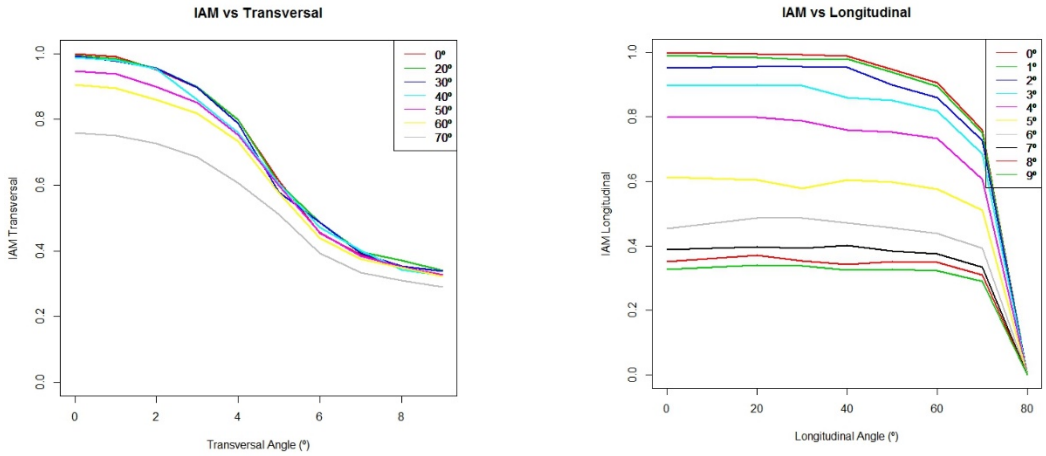

Fig. 8: IAM 2D curves for a CPC solar collector by Tonatiuh

The other simple method is the so called dummy variable or angle by angle method [5], which is a testing method. The theory is that by dividing the beam irradiance into several terms according to the pre-setting incident angle intervals, like 15° in the following table, the measured beam irradiance is put into the corresponding column and other beam irradiance columns are set to 0. Then the mathematical model can be revised as Eq. (15). $K_b(\vartheta)$ can be obtained by the regression calculation together with other parameters at the same time. Therefore, it is a convenient method for getting IAM. Of course, smaller incident angle intervals can increase the precision of the regressed IAM.

Table 1 An example of angle by angle method [5]

G_b (0°-15°) *W/m²*	G_b (15°-30°) *W/m²*	G_b (30°-45°) *W/m²*	G_b (45°-60°) *W/m²*	G_b (60°-75°) *W/m²*	G_b (75°-90°) *W/m²*	G_d *W/m²*	$(T_f - T_a)$ *K*	$(T_f - T_a)^2$ *K²*	$dT_f / d\tau$ *K/s*
0	0	0	0	0	200	200	10	100	0.001
0	0	0	0	230	0	300	20	400	0.002
0	0	0	400	0	0	150	34	1156	0.004
0	0	560	0	0	0	167	48	2304	0.003
0	800	0	0	0	0	120	50	2500	0.005
567	0	0	0	0	0	170	47	2209	-0.001
0	340	0	0	0	0	200	38	1444	-0.002
0	0	100	0	0	0	250	32	1024	-0.002
0	0	0	50	0	0	120	20	400	-0.001

0	0	0	0	172	0	189	22	484	0.001
0	0	0	0	0	204	260	28	784	0.001

$$q_u = \eta_0 K_b\left(0^\circ\text{-}15^\circ\right) S_b G_b\left(0^\circ\text{-}15^\circ\right) + \eta_0 K_b\left(15^\circ\text{-}30^\circ\right) S_b G_b\left(15^\circ\text{-}30^\circ\right) + \cdots + \eta_0 K_b\left(75^\circ\text{-}90^\circ\right) S_b G_b\left(75^\circ\text{-}90^\circ\right)$$
$$+\eta_0 K_d S_d G_d - a_1(T_f - T_a) - a_2(T_f - T_a)^2 - a_3 u(T_f - T_a) + a_4(E_L - \sigma T_A{}^4) - a_5 dT_f / dt - a_6 uG \quad (15)$$

5. In situ test method

Typical layout

The layout of solar collector fields is typically array parallel connections. Solar collectors are connected in series as an array. The arrays are deployed in parallel as a matrix. All the outlet of the arrays are gathered in manifolds. Usually, the number of solar collectors in each array is the same in order to get similar outlet temperature at the end of the array. Therefore, for small or medium solar collector field, the layout of solar collectors is often seen as rectangle, like Fig. 9 shown. But for large solar collector field, due to different local topography, the layout of solar collectors could be flexible. Fig. 10 shows the current world largest solar collector field in Silkeborg, Denmark with a solar collector area of 156.000 m^2. The solar collector field is composed of several rectangle collector matrixes together with several irregular collector matrixes. The layout of solar collector field is still array parallel style. But each array could have different number of solar collectors because of the limitation of topography. The outlet temperature can be anticipated or adjusted by the number of solar collectors and the flow rate in arrays. Volume flow rate per square meter collector area is typically constant for all rows resulting in the same outlet temperature for each row.

Fig. 9: Solar district heating for 3,000 households in the German town of Senftenberg [10]

Fig. 10: Solar heating plant in Silkeborg, Denmark [11]

Array monitoring and field monitoring

The in situ monitoring system can be implemented for one array or several arrays of the solar collector field or the whole solar collector field. This can be decided by the complexity of installation according to local conditions. The monitored data should include the total and diffuse solar radiation on the collector plane, the inlet and outlet temperatures of the targeted array/arrays/field, the flow rate and the ambient temperature. For tracking solar collectors, monitoring the beam radiation could be considered as necessary and the collector tilt monitoring is mandatory. The data log time interval can be decided by the capability of the monitoring system. But a short time interval such as less than 1 min is recommended.

In situ test method

The in situ test method includes two procedures. The first is the parameter identification and the other is the thermal performance prediction. Both of them use the modified QDT mathematical model as the control equation, which is shown as Eq. (1).

The aim of parameter identification is to obtain the model parameters such as the maximum efficiency, heat loss coefficients, incident angle modifier, etc. which can be used to evaluate the investigated solar collector field and to predict the thermal performance of solar collector field in short and long term.

Multi Linear Regression [6] is needed for obtain the model parameters.

The thermal performance prediction is the reverse process of the parameter identification. Based on the model parameters, the operating conditions and weather conditions, the useful heat output is calculated.

The thermal performance prediction can be calculated by real operating data and weather data or by standard operating conditions and typical weather conditions at different locations. The latter method can be used for calculating annul thermal performance prediction under standard operation and weather conditions. The results can be used for comparing the solar collector field thermal performance at different locations which can be referenced for planning of new solar collector fields. The in situ test method is a good way for providing an accurate and reliable thermal performance prediction.

The shading model and incident angle modifier method describe in section 3 and section 4 should be implemented for both the parameter identification and thermal performance prediction.

The equations or relations for calculating solar angles, solar radiation and Sun-collector geometric relation can reference the literature [12].

6. Experimental verification

In order to validate the mathematical model and the in situ test method, two experimental case studies are carried out. The two experimental verifications focus on flat plate solar collector field operating in Denmark and in situ monitored data were used. The first case monitored one collector array in the collector field and the other monitored the whole collector field. The model parameters were derived by implementing Eq. (1) and the experimental data, which are compared to the standard lab test results. Then the predicted heat output for the whole collector field were compared to the measured heat output under the measured operating and weather conditions. The conclusion can be made that the in situ test method is valid and can accurately predict the thermal performance of the solar collector fields.

Case study 1 – Flat plate solar collector field in Sæby solar heating plant

Fig. 11 and Fig. 12 show the solar heating plant in Sæby, Denmark that is located at latitude: 57.32 °N and longitude 10.5 °E. The solar heating plant has 863 flat plate solar collectors forming an 11866 m^2 (aperture area) solar collector field. The solar collectors were provided by Sunmark A/S with a length of 5.69 m, width of 2.52 m and the gross area of 15.02 m^2. The technical data from lab test results is shown in Table 2.

The solar collector field has a total of 53 rows with a row distance of 6 m and a slope of 30 °. The collectors are facing south with 8 ° towards west. The heat transfer fluid going through the whole collector field is glycol/water mixture (39%/61% in weight).

Four flat plate solar collectors in the last row of the solar collector field were monitored starting from May 2017. The inlet and outlet temperatures, the flow rate, the ambient temperature and the total and diffuse solar irradiance on the collectors were recorded every 10 seconds since then.

Fig. 11: Aerial view of Sæby solar heating plant

Fig. 12: Solar collector arrays in Sæby solar heating plants

The collector or collector array tested parameters comparison is shown in Table 2. The lab test results were taken from standard test report [13]. The in situ test results were tested from the monitored data of June 2017. From the comparison it can be seen that the maximum efficiency of in situ test is lower than the lab test result while the heat loss coefficient is higher. Possible reasons are that the single collector tests at the test lab gave too optimistic results, that the heat losses from pipes in the solar collector loop are not considered, that dirt is attached to the cover glass, and that moisture are present inside the

collectors. No matter in what, it demonstrated that the in situ operation was different from the lab test conditions. With regards to which results are more reasonable for predicting the thermal performance of solar collector field, the experimental verification is carried out as follows.

Table 2 Model parameter comparison

Collector (array) parameters	Lab test, from test report (single collector)	In situ test (four collectors' array)
Maximum efficiency η_0 (-)	0.815	0.769
Direct IAM coeff. b_0 (-)	0.11	0.22
Diffuse IAM K_d (-)	0.90	0.93
Heat losses a_1 (W/m^2K)	3.43	4.63
Heat losses a_2 (W/m^2K^2)	0.0145	0
Effective capacity a_5 (J/m^2K)	8028	6683

Fig. 13 shows a typical sunny day thermal performance comparison. The blue curve is the measured power output of the collector array. The orange and green curves are predicted collector array power output. The orange curve was calculated by using the lab test collector parameters while the green curve using the in situ test results. It is that the green curve coincides well with the blue curve while the orange curve has a larger deviation compared to the blue curve. The figure demonstrates that by using the in situ test collector array parameters, the thermal performance of the collector field can be precisely predicted. Fig. 14 shows a partly cloudy day thermal performance comparison and Fig. 15 and Fig. 16 show cloudy days' thermal performance comparison, which all have the same consequence. The figures give a visual daily comparison on the two predicted methods and a concrete conclusion can be made that the thermal performance of the solar collector field can be accurately modelled by the modified QDT model and that the in situ test method is better than lab test method for this purpose.

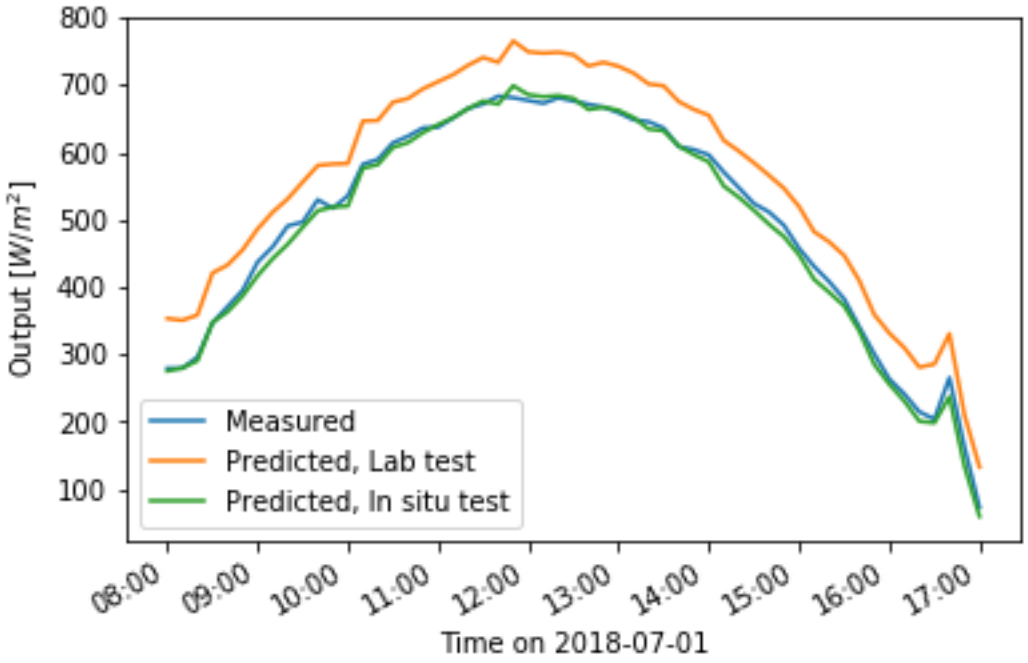

Fig. 13: Measured and predicted power output comparison on 01-07-2018

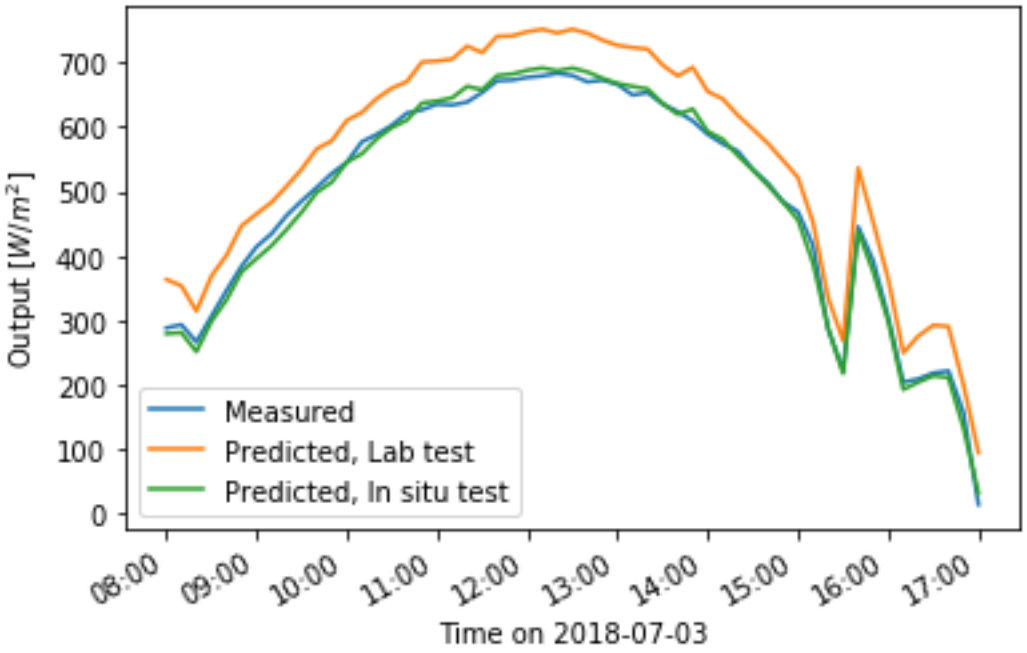

Fig. 14: Measured and predicted power output comparison on 03-07-2018

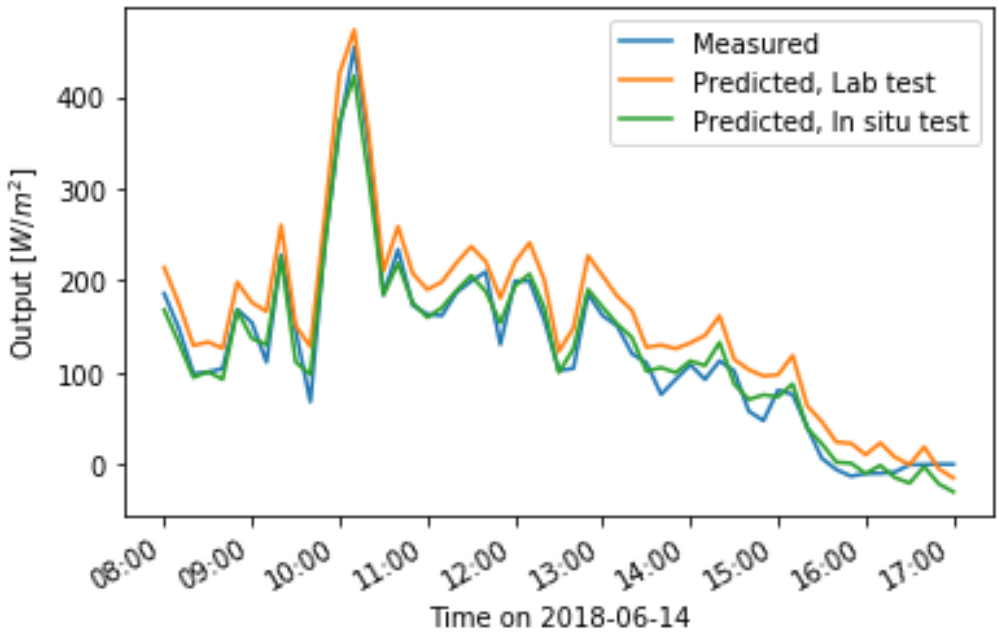

Fig. 15: Measured and predicted power output comparison on 14-06-2018

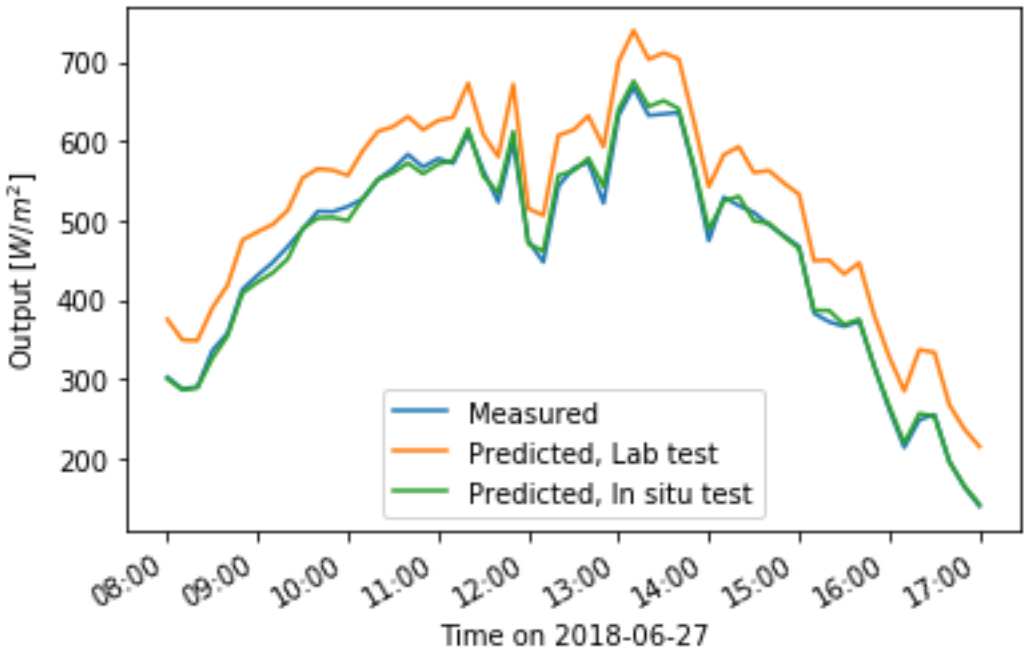

Fig. 16: Measured and predicted power output comparison on 27-06-2018

Table 3 gives the monthly comparison for the different test methods. The test period was from December 2017 to June 2018. Due to some technical problems, not all days' data of all months were recorded. The second column lists the days recorded in each month. Of course, all the measured and modelled results were taken from the same days in each month. The total and diffuse solar radiation on the collector array is shown in column 3 and 4. Then followed by the measured heat output and modelled heat output using lab test collector parameters and in situ test parameters, separately. The last column is the measured heat output obtained from the website solvarmedata.dk, which is an online database monitoring most of the solar heating plants in Denmark. The data from the last column was measured for the whole solar collector field. The last row is the summation of each column.

From the table it can be seen that for the period of 153 days, the total solar radiation on the collector array is 581 kWh/m^2, of which 155 kWh/m^2 is diffuse radiation. The measured heat output of the collector array is 286 kWh/m^2 while the modelled heat output are 364 and 309 kWh/m^2, by using lab test result and in situ test result respectively. The measured heat output for the whole solar collector field is 274 kWh/m^2. The two measured summation results are quite close which means the collector array performs similar to the whole solar collector field. The modelled heat output by using the in situ test is also close to the measured heat output. The modelled heat output by using the lab test results has a larger deviation compared to the measured heat output. The comparison shows that the in situ test method and the modified QDT mathematical model are good enough to predict the thermal performance of solar collector field.

Table 3 Monthly measured and modelled heat output comparison

Flat plate collector / Month	Measured days	Total solar radiation on collector array	Diffuse solar radiation	Measured heat output	Modelled heat output, Lab test	Modelled heat output, In situ test	Measured heat output (whole plant, from solvarmedata.dk)
		(kWh/m^2)	(kWh/m^2)	(kWh/m^2)	(kWh/m^2)	(kWh/m^2)	(kWh/m^2)
12. 2017	9	2	2	0	1	1	0
01. 2018	9	2	1	0	1	0	0
02. 2018	26	38	13	5	9	6	3
03. 2018	19	62	13	20	25	20	24
04. 2018	29	122	36	51	63	51	51
05. 2018	31	209	40	106	133	114	100
06. 2018	30	209	49	104	133	117	96
Sum	**153**	581	155	286	364	309	274

Case study 2 – Flat plate solar collector field in Tårs solar heating plant

Figs. 17 and 18 show the hybrid solar heating plant with a 5960 m^2 flat plate collector field and a 4039 m^2 parabolic trough collector field in series in Tårs, Denmark (latitude: 57.39 °N, longitude: 10.11 °E). The plant was put into operation in August 2015.

Fig. 19 briefly illustrates the basic principle of the solar heating plant. The solar collector fluid for the parabolic trough collectors is water, while that in the flat plate solar collector is a glycol/water mixture (35%/65% in weight). The return water from the district heating network is heated up to 65–75 °C by the heat exchanger connected to the flat plate collector field. Then the preheated water from the flat plate collector field is heated to the required temperature by going through the parabolic trough collector field. The orientation of parabolic trough collector axes was 13.4° towards west from south. The parabolic trough collectors track the sun from east to west when the collectors work during the whole day. There are six rows of parabolic trough collectors and the row distance is 12.6 m. The length of each row of the parabolic trough collector loop is about 125 m. The orientation of the flat plate collectors is due south and the collector row distance is 5.67 m. The tilt of the flat plate collectors is 50°. The flat plate collector field consist of two types of collectors, namely HTHEATboost 35/10 and HTHEATstore 35/10, manufactured by Arcon-Sunmark A/S. Half of the flat plate collector field is made of HTHEATboost 35/10, while the other half is of HTHEATstore 35/10 [14]. Technical data on the flat plate solar collectors and collector field can be found in Table 4.

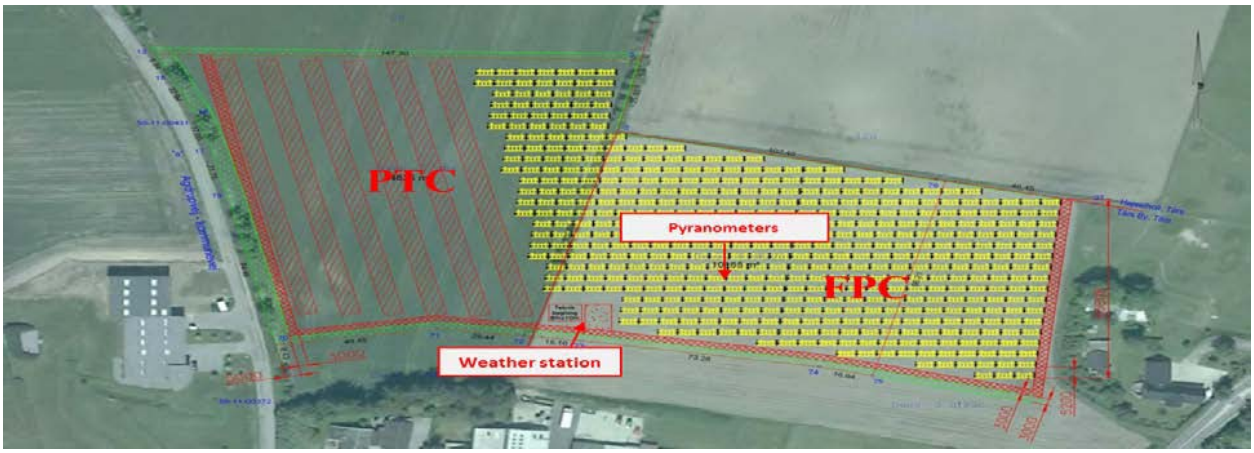

Fig. 17: Layout of solar collector field in Tårs solar heating plant

Fig. 18: solar collector arrays in Tårs solar heating plant

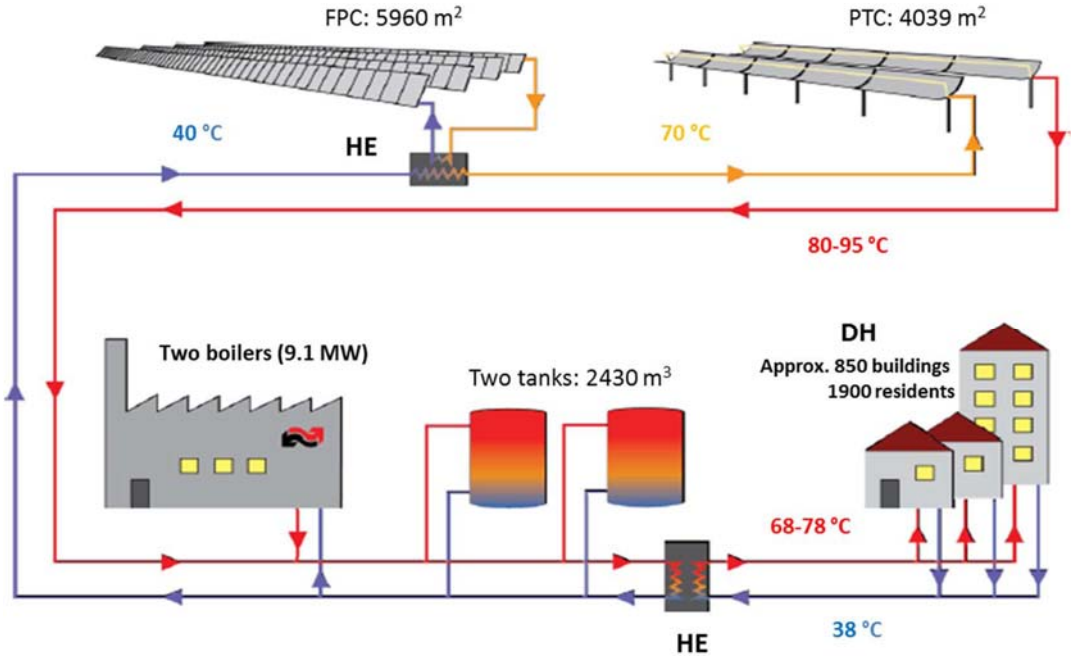

Fig. 19: schematic diagram of operation principle of Tårs solar heating plant

Table 4. Information on solar collector and solar collector field

Flat plate collector		Flat plate collector field	
Aperture area [m^2]	12.60	Aperture area [m^2]	5960
Gross area [m^2]	13.57	Gross area [m^2]	6419
Length [m]	5.96	Row distance [m]	5.67
Width [m]	2.27	Rows [-]	39
Tilt [°]	50	Collector in Row	Typically 6 flat plate collectors without foil and 6 flat plate collectors with foil

Investigations on in situ test of solar collector field will only focus on flat plate solar collector field. The lab test results for the two types of flat plate solar collectors can be seen in Table 5 [14]. The results were taken from standard test sheet based on gross collector area. It can be seen from the table that the flat plate collector with foil has a lower maximum efficiency but also a lower heat loss coefficient than the collector without foil, which is consistent with the expectations.

The in situ model parameters test for the solar collector field was carried out from January 2017 to June 2017. The monitoring system is well equipped with different accurate sensors and the monitoring data are automatically transferred to the computers. Global solar radiation on the horizontal surface and total radiation on the tilted flat plate collectors are measured with Kipp & Zonen SMP11. DNI is measured with a PMO6-CC pyrheliometer with the sun tracking platform Sunscanner SC1. The inlet and outlet temperatures of the collector fields are measured with SIEMENS TS500 temperature sensors, flow rates of both the FPC field and the PTC field are measured with Sitrans FM MAG3100P flow meters - SIEMENS. Measured thermal performance is calculated based on the measured parameters.

The inlet temperature, outlet temperature and flow rate data for the flat plate collector field were taken from the heat exchanger side. Therefore, the whole flat plate solar collector field was monitored during that period. The monitoring time interval is 2 min.

The in situ test results for the whole solar collector field is also shown in Table 5 as the last column. The field is assumed only to have one collector type. It can be seen from the table that the maximum efficiency of the in situ test result is lower than the two collectors' lab test results, which verified the basic argument of the in situ test method that the maximum efficiency of solar collector fields will be lower than the single collector lab testing. Therefore, the thermal performance prediction by the in situ test method will be more precise than using the parameter data extracted from single collector test report. The heat loss coefficient, diffuse IAM are close to lab test results while the direct IAM and effective capacity have bigger differences compared to the lab test results.

Table 5. Model parameter comparison

Parameter	HTHEATboost Lab test	HTHEATstore Lab test	Flat plate collector field in situ test
Maximum efficiency η_0 (-)	0.779	0.745	0.706
Direct IAM coeff. b_0 (-)	0.1	0.1	0.24

Diffuse IAM K_d (-)	0.98	0.93	0.78
Heat losses a_1 (W/m^2K)	2.41	2.07	2.14
Heat losses a_2 (W/m^2K^2)	0.015	0.009	0
Effective capacity a_5 (J/m^2K)	6798	7313	3694

The thermal performance prediction was carried out for the whole year of 2016 according to the mathematical model of Eq. (1). The shading effect and incident angle modifier were also calculated based on the deployment of flat plate collector field. The measured useful power output was calculated by the monitored data. The predicted useful power output was calculated by the lab test collector parameters and in situ test collector field parameters separately, together with the measured weather condition and flow rates.

The measured and predicted useful power output comparison for the whole collector field is shown in single day figures and monthly sums for the whole year 2016. Fig. 20 shows a typical sunny day comparison between measured and predicted power output. The blue curve is the measured power output. The orange curve is the predicted power output using lab test collector parameters while the green is the predicted power output using the in situ test collector field parameters. The orange curve coincides well with the blue curve during the noon period while the green curve fits the blue curve better during the morning and afternoon period. Fig. 21 shows a partly cloudy day comparison and Figs. 22 and 23 show two cloudy day comparisons for the measured and predicted power output. It can be seen from figures that the predicted power output by using lab test results are close to the measured power output mainly in noon periods while the predicted power output using the in situ test collector field parameters are more close to the measured power output mainly in the morning and afternoon period. That is, the lab test results for single solar collector are quite good. But maybe due to the strict QDT test requirements for single collector, the test results can't fit for the whole day period. This could be a hint for further improvement for the QDT single collector test method. The in situ test result seems having bigger difference during noon period compared to the measured result but the result was optimized by minimizing the errors for the whole days, which was verified by the monthly sums in Table 6.

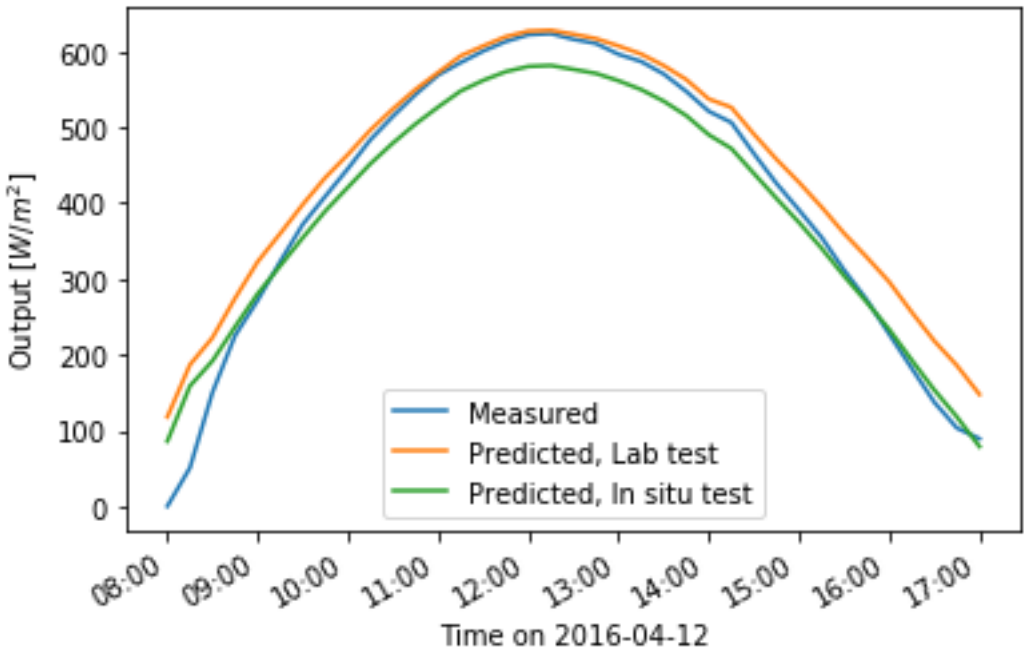

Fig. 20: Measured and predicted power output comparison on 12-04-2016

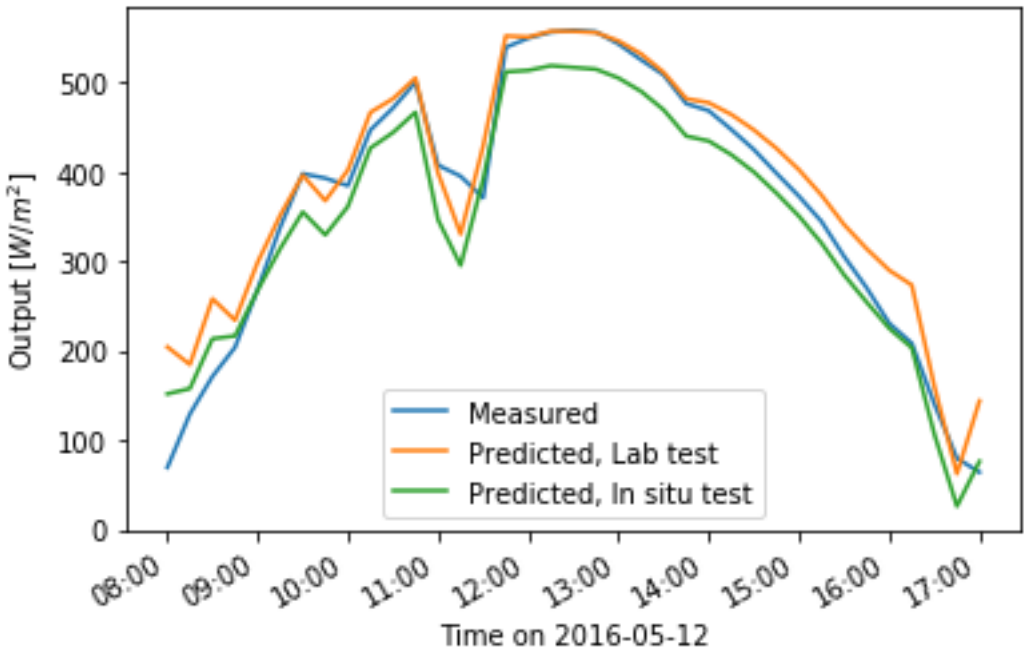

Fig. 21: Measured and predicted power output comparison on 12-05-2016

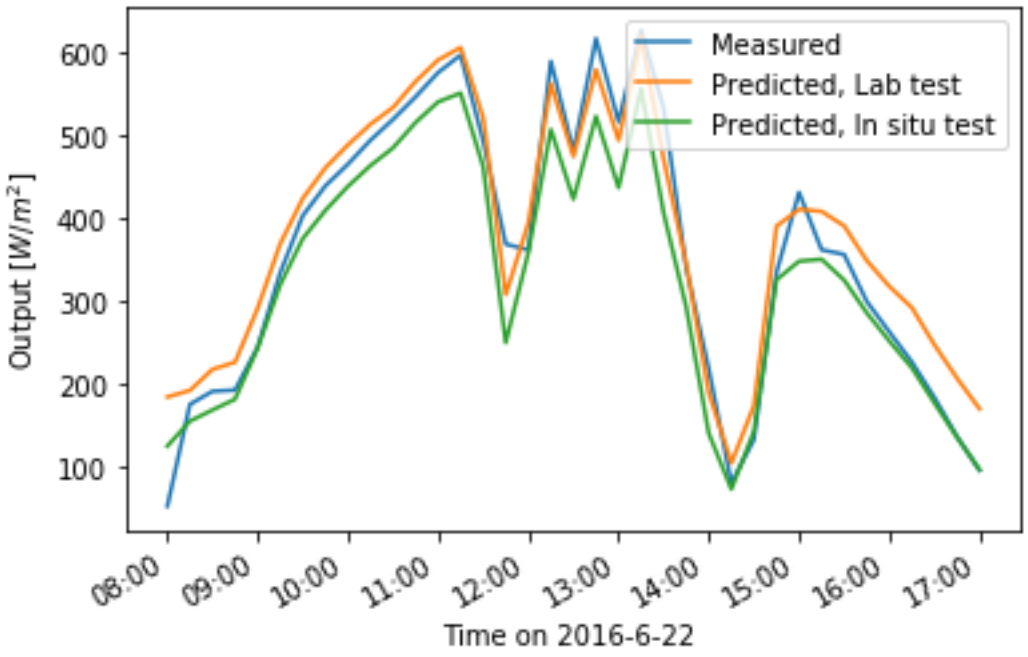

Fig. 22: Measured and predicted power output comparison on 22-06-2016

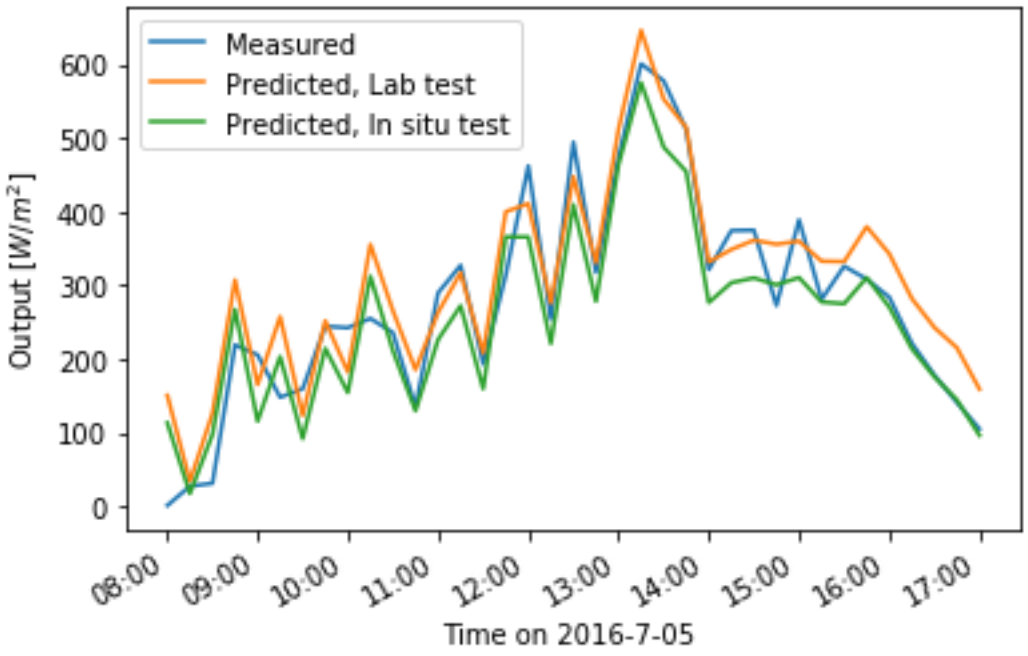

Fig. 23: Measured and predicted power output comparison on 05-07-2016

Table 6 shows the monthly sums of solar radiation and collector field heat output for the whole year of 2016. The total solar radiation and diffuse solar radiation are listed in column 3 and 4, followed by the

measured heat output, modelled heat output using lab test parameters and modelled heat output using in situ test parameters. The last row is the sum of each column.

From the table it can be seen that for the whole year, the total solar radiation on flat plate collector field is 1185 kWh/m^2 while 550 kWh/m^2 was contributed by diffuse solar radiation. The measured heat output of the collector field is 411 kWh/m^2, which is quite close to the modelled heat output by using the in situ test results, 407 kWh/m^2. However, the modelled heat output by using the lab test results is 486 kWh/m^2, which has a larger deviation compared to the measured heat output. The monthly comparison results clearly demonstrate that the in situ test method can predict more precise the heat output for the solar collector field thermal performance compared to the method just using the collector parameters tested from lab.

Table 6. Monthly measured and modelled heat output comparison

Flat plate collector/ Month	Measured days	Total solar radiation on collector field (kWh/m^2)	Diffuse solar radiation (kWh/m^2)	Measured heat output (kWh/m^2)	Modelled heat output, Lab test (kWh/m^2)	Modelled heat output, In situ test (kWh/m^2)
01. 2016	31	25	15	2	3	3
02. 2016	28	74	25	21	24	22
03. 2016	31	86	42	28	31	26
04. 2016	30	133	60	48	57	48
05. 2016	31	171	71	67	81	68
06. 2016	30	159	76	60	73	60
07.2016	31	143	85	52	64	51
08.2016	31	142	69	56	65	53
09.2016	30	134	59	56	60	51
10.2016	31	60	22	19	23	20
11.2016	31	33	16	3	5	4
12.2016	30	24	10	1	2	2
Sum	**365**	**1185**	**550**	**411**	**486**	**407**

Discussion

There are several test methods developed for evaluating the thermal performance of solar collector field. The most detailed way is the TRNSYS simulation. But creating a detailed TRNSYS project is not easy and time consuming. In addition, the TRNSYS project cannot be used for other solar heating plants directly. Other simple mathematical models like the quasi-stationary method or guaranteed power output method are a little bit too simple and they use collector standard test results.

The developed in situ method uses the modified QDT mathematical model, which is a relative simple model with high accuracy and considers the shading effect in solar collector field. Further, it uses in situ test results for evaluating the thermal performance of solar collector field.

By using the in situ test method, the pipe heat losses are considered inherently. The real operating conditions of solar collectors in the field are reflected. In addition, the in situ method uses the weather data from radiation sensors in the field which is an important factor to get accurate results.

Conclusions

An in situ test method for evaluating and predicting the thermal performance of solar collector field is developed. The mathematical model of the in situ test method is improved from the QDT test model, which is mainly used for single solar collector testing. The difference of single collector testing and collector field testing is discussed and the detailed shading models for different kinds of solar collectors are also developed. Methods of getting different collectors' incident angle modifiers are listed. Two experimental verifications were carried out. The model parameters derived by using the in situ test method were compared to that by using lab test results. The predicted thermal performance of the solar collector field were calculated both by the in situ test model parameters and the lab test results. The predicted thermal performance and the measured thermal performance were compared both for single days and for months. The predicted thermal performance by the in situ test method is closer to the measured thermal performance than the predicted thermal performance by the lab test results.

Acknowledgement

The work was funded and supported by the Bjarne Saxhofs Fond (project 26675).

References

[1] "Solar heating plants in Denmark." [Online]. Available: http://solar-district-heating.eu/ServicesTools/Plantdatabase.aspx.

[2] F. Bava and S. Furbo, "Development and validation of a detailed TRNSYS-Matlab model for large solar collector fields for district heating applications," *Energy*, vol. 135, pp. 698–708, 2017.

[3] J. E. Nielsen, "Quasi-dynamic model for simulation of large solar collector fields," 2016. [Online]. Available: http://www.solarthermalworld.org/sites/gstec/files/news/file/2016-12-07/jan_erik_nielsen.pdf.

[4] J. E. Nielsen, "Personal contact." .

[5] B. Perers, "An improved dynamic solar collector test method for determination of non-linear optical and thermal characteristics with multiple regression," *Sol. Energy*, vol. 59, pp. 163–178, 1997.

[6] S. Fischer, W. Heidemann, H. Muller-Steinhagen, B. Perers, P. Bergquist, and B. Hellstrom, "Collector test method under quasi-dynamic conditions according to the European Standard EN 12975-2," *Sol. Energy*, vol. 76, pp. 117–123, 2004.

[7] "ISO 9806 Solar energy- Solar thermal collectors -Test methods." International Standards Organization, Geneva, Switzerland, 2013.

[8] E. Zambolin and D. del Col, “An improved procedure for the experimental characterization of optical efficiency in evacuated tube solar collectors,” *Renew. Energy*, vol. 43, pp. 37–46, 2012.

[9] M. J. Blanco, J. M. Amieva, and A. Mancillas, “The Tonatiuh Software Development Project: An Open Source Approach to the Simulation of Solar Concentrating Systems,” no. 42142. pp. 157–164, 2005.

[10] “https://www.solarthermalworld.org/content/solar-district-heating-3000-households-german-town-senftenberg.” .

[11] “https://ing.dk/artikel/verdens-stoerste-solfangeranlaeg-drift-silkeborg-191730.” .

[12] J. a Duffie and W. a. Beckman, “Solar Engineering of Thermal Processes-Second Edition,” p. 469, 1980.

[13] “www.estif.org/solarkeymark/Links/Internal_links/SP/509301.pdf.” .

[14] Z. Tian, B. Perers, S. Furbo, and J. Fan, “Annual measured and simulated thermal performance analysis of a hybrid solar district heating plant with fl at plate collectors and parabolic trough collectors in series,” *Appl. Energy*, vol. 205, no. July, pp. 417–427, 2017.